Time-periodic Klein-Gordon media: Tunable wave-vector gaps and Dirac dispersion with an exceptional point of degeneracy

A. Paliovaios, V. Achilleos, Georgios Theocharis, D. Frantzeskakis, N. Stefanou

Time-Periodic Klein-Gordon Media: Tunable Wavevector Gaps and Dirac Dispersion with Exceptional Point of Degeneracy

A. Paliovaios,[1,2] V. Achilleos,[1] G. Theocharis,[1] D. Frantzeskakis,[2] and N. Stefanou[2]

[1] *Laboratoire d'Acoustique de l'Université du Mans (LAUM), UMR 6613, Institut d'Acoustique - Graduate School (IA-GS), CNRS, Le Mans Université, France*

[2] *Section of Condensed Matter Physics, National and Kapodistrian University of Athens, University Campus, GR-157 84 Athens, Greece*

(Dated: November 25, 2024)

The present study delves into the exploration of wave propagation in spatially homogeneous systems governed by a Klein-Gordon-type equation with a periodically time-varying cutoff frequency. Through a combination of analytical calculations and numerical simulations, intriguing and distinctive features in the dispersion diagram of these systems are uncovered. Unlike other systems with spatial and temporal periodicity, the examined configurations demonstrate some remarkable transitions as the modulation frequency increases. These transitions encompass a transformation from a frequency gap to a wavenumber gap around $q = 0$, with the transition point corresponding to a gapless Dirac dispersion with exceptional point of degeneracy. Subsequently, the q-gap undergoes a bifurcation into two symmetric gaps at positive and negative wavenumbers. At this second transition point, the dispersion diagram takes the form of an imaginary Dirac dispersion relation and exhibits an isolated exceptional point at the center of the q=0 gap. These findings contribute to a deeper understanding of wave dynamics in periodically modulated media, uncovering novel and tunable phenomena.

I. INTRODUCTION

The Klein-Gordon equation [1, 2] in quantum physics offers a fundamental description of relativistic spinless particles through a scalar field. Its mathematical form, akin to the d' Alembert wave equation with an additional term proportional to the field, introduces a spectral cutoff for propagating waves. Interestingly, this equation finds relevance in classical systems as well. For example, in 1909, Lamb derived a similar equation to describe vertically propagating acoustic waves in the atmosphere [3]. Today, Klein-Gordon-type equations have become integral in diverse fields, modeling phenomena such as propagation of electromagnetic waves in waveguides [4] and plasmas [5], Alfvén waves in nonuniform media [6], duct acoustics [7], vibrating strings [8], upward propagation of linear acoustic waves in a gravitationally stratified solar atmosphere [9], etc.

In recent years, the pursuit of innovative wave applications, encompassing magnetless nonreciprocity, multimode shaping, parametric amplification, and ultrafast switching, has reignited interest in time-varying media [10]. Particularly, media with properties that vary periodically over time exhibit wavevector gaps [11–13], analogous to the frequency gaps occurring in spatially periodic structures [14–16]. In a wavevector gap, only complex-frequency solutions of the wave equation exist. These solutions come in pairs and represent modes with amplitudes that either grow or decay exponentially. Both options are physically acceptable, in sharp contrast to frequency gap modes where energy conservation prevents the existence of waves with growing amplitude in the medium.

In parallel to the studies on spatially or temporally periodic media which can host only one type of gap, subject of study is spatiotemporally periodic media, too. In this context, the band structure and the associated field eigenmodes have mainly been explored under the assumption of a travelling wave modulation, in the absence of which the system is dispersionless [17–20]. This scenario, depending on modulation's phase velocity leads either to frequency or wavevector gaps. The transition from frequency to wavevector gap (and vice versa) occurs when phase velocity is equal to wave propagation velocity. However, at the transition point all the modes of the unmodulated system are strongly coupled making its study rather challenging [18, 19].

While extensive research has been conducted on periodic systems and their dispersion properties concerning wave propagation, the interplay between frequency and wavevector gaps has received comparatively less attention [21, 22]. What is more, within most of the available studies, frequency gaps emerge from spatial periodicity, leaving the influence of temporal modulation on the properties of spatially homogeneous media, which inherently possess frequency gaps, largely unexplored. Only recently, an electromagnetic waveguide loaded with a one-dimensional lattice of coupled time-periodically driven LC resonators, an inherently gapped system, was considered [23].

In the present paper, we report a thorough theoretical investigation into the interplay between the intrinsic frequency gap of a homogeneous medium and the wavevector gaps arising from a temporal modulation. The wave propagation in our study adheres to the generic Klein-Gordon equation with a periodically varying cutoff frequency. As a result, Klein-Gordon-type systems allow us to explore the interplay between frequency and wavevector gaps without assuming any specific form of spatiotemporal modulation but rather focusing on a gen-

eral time-periodic drive, thus departing from previous assumptions [22].

The remainder of the paper is structured as follows. In Section II, we present our theoretical framework. This section lays the groundwork for our analysis by establishing the fundamental principles upon which our study is built. Following this, in Section III, we develop a perturbative approach. This method enables us to accurately describe our results in a simple yet consistent manner, facilitating a deeper understanding of the phenomena under investigation. Section IV is dedicated to the systematic analysis of dispersion diagrams as they evolve with modulation frequency. Here, we uncover unique characteristics, including Dirac dispersion, in both real and imaginary space, with exceptional point of degeneracy, and wavenumber gaps around $q = 0$. Next, in Section V, we delve into a numerical study of the wave properties of time-modulated Klein-Gordon media. Our primary focus is on the case of Dirac dispersion relation with exceptional point of degeneracy. Through this analysis, we illuminate the unusual dynamics that emerge, demonstrating the accuracy of our theoretical framework in describing these phenomena. Finally, the paper concludes in the last section, where we summarize our findings.

II. THEORETICAL FRAMEWORK

We start from a wave equation of the general Klein-Gordon form in a single spatial dimension

$$\left(\frac{\partial^2}{\partial t^2} - c^2\frac{\partial^2}{\partial x^2} + \widetilde{\omega}_c^2\right) u(x,t) = 0\ , \tag{1}$$

where c, $\widetilde{\omega}_c$ are positive constants and $u(x,t)$ is a field, the nature of which depends on the physical system under consideration. This equation type reveals a spectral gap for propagating waves, ranging from $-\widetilde{\omega}_c$ to $\widetilde{\omega}_c$. Consequently, $\widetilde{\omega}_c$ is designated as the cutoff frequency.

In contrast to the common approach of temporally modulating the constant c, which, in dispersionless systems, represents the wave propagation velocity, here, we choose to vary the cutoff frequency $\widetilde{\omega}_c$. Specifically, we assume that

$$\widetilde{\omega}_c^2 = \omega_c^2[1 + \varepsilon\cos(\Omega t)], \tag{2}$$

where ε, Ω are the (relative) amplitude and the frequency of the modulation, respectively. Under this assumption, Eq. (1) takes the form

$$\left(\frac{\partial^2}{\partial t^2} - c^2\frac{\partial^2}{\partial x^2} + \omega_c^2\right) u(x,t) + \omega_c^2\varepsilon\cos(\Omega t)u(x,t) = 0\ , \tag{3}$$

which describes a homogeneous system under the effect of a periodic uniform modulation, of period $T = 2\pi/\Omega$. As we will show in Sec. IV, periodic time variations of c in the Klein-Gordon equation do not lead to the same rich wave phenomenology.

Taking advantage of the spatial homogeneity of Eq.(3), we utilize a Fourier expansion for the general solution with $u_q(t) = \int_{-\infty}^{\infty} dx u(x,t)\exp(-iqx)$, thus ensuring that each Fourier component complies with a Mathieu's equation

$$\frac{d^2u_q}{dt^2} + \left[c^2q^2 + \omega_c^2 + \omega_c^2\varepsilon\cos(\Omega t)\right] u_q = 0. \tag{4}$$

According to Floquet theory, the solutions of Eq. (4) can be written in the form [24]

$$u_q(t) = e^{-i\omega t}\phi(t), \tag{5}$$

where $\phi(t+T) = \phi(t)$. It is worth noting that the Floquet exponent, ω, is not unique, as Floquet exponents which differ by an integer multiple of Ω correspond to an equivalent solution. In practical terms, this means that we can focus on a specific interval of the real part of ω within a range of Ω. This interval is often confined to the first Brillouin zone, represented as $(-\Omega/2, \Omega/2]$.

In certain regions of the wavenumber q, referred to as wavenumber gaps, the Floquet exponents form complex conjugate pairs, signifying two linearly independent solutions of Eq. (4): one exponentially growing and one exponentially decaying in time. Outside these complex regions, the linearly independent solutions correspond to real-valued ω with opposite signs and consequently to two periodic stable solutions. However, exceptions occur at the center and the edges of the first Brillouin zone, where the two solutions can coalesce [25–28], creating what is known as exceptional points. The existence of an exceptional point gives rise to one periodic stable and one linearly growing in time solution.

Because of the periodicity of $\phi(t)$, we express it as a Fourier series, resulting in

$$\phi(t) = \sum_{n=-\infty}^{\infty} w_n e^{in\Omega t}. \tag{6}$$

By substituting Eq. (5) along with the expansion from Eq. (6) into Eq. (4), we obtain

$$\left[c^2q^2 + \omega_c^2 - (\omega - n\Omega)^2\right] w_n + \frac{\omega_c^2\varepsilon}{2}(w_{n+1} + w_{n-1}) = 0\ , \tag{7}$$

which can be cast in the form of a quadratic eigenvalue problem

$$\left[\omega_\nu^2\mathbf{I} + \omega_\nu\mathbf{A} + (\mathbf{B} + \varepsilon\mathbf{P})\right]\overrightarrow{w}_\nu = 0\ , \tag{8}$$

where ω_ν is the ν-th eigenvalue and $\overrightarrow{w}_\nu$ is a column vector which contains the Fourier coefficients $w_{\nu;n}$ of the ν-th eigenmode. $\mathbf{I}$ is the unit matrix, $\mathbf{A}$ and $\mathbf{B}$ are diagonal matrices with elements $A_{mn} = -2m\Omega\delta_{mn}$ and $B_{mn} = (m^2\Omega^2 - \omega_c^2 - c^2q^2)\delta_{mn}$, respectively, while $\mathbf{P}$ is a Toeplitz tridiagonal matrix with elements $P_{mn} = -\omega_c^2(\delta_{mn+1} + \delta_{mn-1})/2$, with δ_{mn} being the Kronecker delta. Equation (8) yields Floquet eigenmodes in the repeated zone scheme, encompassing linearly independent

solutions in the first Brillouin zone and equivalent solutions outside it, with corresponding ω values differing by integer multiples of Ω.

It is important to note that, at an exceptional point, Eq. (7) provides only one of the two linearly independent Floquet solutions, represented as $u_{1;q}(t) = \exp(-i\omega t)\phi_1(t)$. However, according to the theory of second-order differential equations with periodic coefficients [29], the second linearly independent solution is given by

$$u_{2;q}(t) = e^{-i\omega t}\left[\phi_2(t) + \frac{t}{T\rho}\phi_1(t)\right], \tag{9}$$

where $\rho = \exp(-i\omega T)$. By substituting Eq. (9) into Eq. (4) and utilizing the expansion from Eq. (6), we determine that $w_{2;n}$ satisfy the equation

$$\left[\omega^2\mathbf{I} + \omega\mathbf{A} + (\mathbf{B} + \varepsilon\mathbf{P})\right]\overrightarrow{w}_2 = -\frac{i\Omega}{2\pi\rho}(2\omega\mathbf{I}+\mathbf{A})\overrightarrow{w}_1. \tag{10}$$

III. PERTURBATIVE ANALYSIS

We now assume that $\varepsilon\mathbf{P}$ in Eq. (8) represents a small perturbation. This assumption enables us to perturbatively examine the system's properties. To achieve this, we commence with the unmodulated system, extracting the $\mathcal{O}(\varepsilon^0)$ order terms of both eigenvalues and eigenvectors. From Eq. (8) we obtain

$$\omega_{0\nu} = \nu\Omega \pm \sqrt{\omega_c^2 + c^2q^2}, \quad w^{(0)}_{\nu;n} = \delta_{n\nu}. \tag{11}$$

The above eigenvalues correspond to replicas of the usual Klein-Gordon dispersion diagram ($\nu = 0$), which are spectrally shifted by integer multiples of the modulation frequency Ω, as shown in Fig. 1. Note that, within the Klein-Gordon frequency gap, the wavenumber assumes imaginary values, as illustrated in Figs. 1(b) and (d).

To comprehend the effect of the periodic modulation on these dispersion diagrams as well as their systematic evolution by varying the modulation frequency, it proves beneficial to extend the wavenumber into the complex plane, seeking solutions of Eq. (3) in the form $\exp[i(qx - \omega t)]\phi(t)$, for given real frequency ω. In this way, we arrive again at Eq. (7) but now this equation should be viewed as a linear eigenvalue equation which, for a real input value of ω within the first Brillouin zone, yields eigenvalues $\lambda = c^2q^2$. This approach is also relevant to problems involving sources [30], or boundary-value problems such as wave scattering by periodically time-modulated media in confined geometries, like finite slabs [23, 31, 32] and isolated objects [33].

Similar to the approach of the nearly-free-electron model for simple metal crystals [14], in the context of perturbation theory to first order, it is straightforward to show that replicas of the unperturbed dispersion curves with no near degeneracy remain unaffected by the modulation. Conversely, close enough to their crossing points,

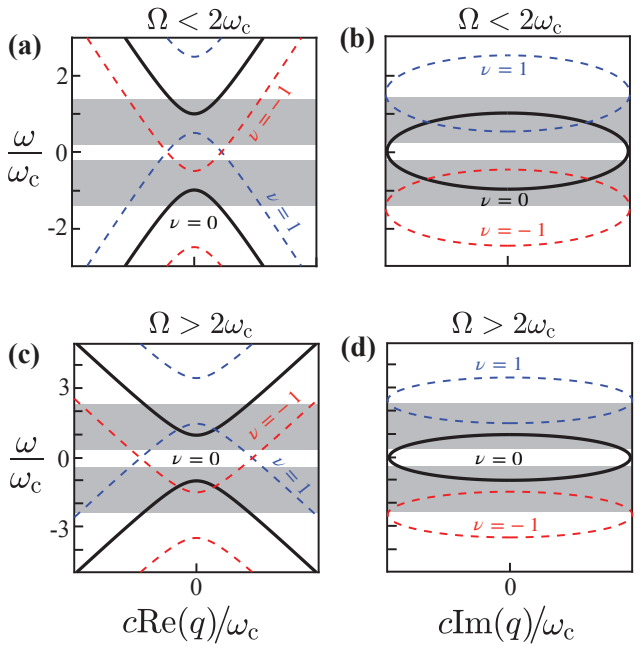

FIG. 1. Schematic representation of the first three replicas of the dispersion diagram for the Klein-Gordon equation [see Eq.(11)] illustrating cases for $\Omega < 2\omega_c$ (a, b) and $\Omega > 2\omega_c$ (c, d). Horizontal gray stripes mark intersections between consecutive replicas where significant mode coupling takes place.

within a range of ε, coupling occurs through the off-diagonal elements of the matrix $\mathbf{P}$. We note that only replicas of orders ν_1 and ν_2, with opposite signs, cross each other. The degeneracy condition (crossing point), $\omega_{0\nu_1} = \omega_{0\nu_2} = (\nu_1 + \nu_2)\Omega/2$, yields

$$\lambda_0 = c^2q_0^2 = \frac{(\nu_2 - \nu_1)^2\Omega^2}{4} - \omega_c^2. \tag{12}$$

In a short range, of order ε, about the degeneracy point, we set $\lambda = \lambda_0 + \varepsilon\lambda_1 + \mathcal{O}(\varepsilon^2)$, where $\lambda_1 = c^2q_1^2$, and Eq. (8) becomes

$$\left[\omega_\nu^2\mathbf{I} + \omega_\nu\mathbf{A} + \mathbf{B}^{(0)} + \varepsilon(\mathbf{B}^{(1)} + \mathbf{P}) + \mathcal{O}(\varepsilon^2)\right]\overrightarrow{w}_\nu = 0 \tag{13}$$

where $B^{(0)}_{mn} = (m^2\Omega^2 - \omega_c^2 - c^2q_0^2)\delta_{mn}$ and $B^{(1)}_{mn} = -c^2q_1^2\delta_{mn}$. By substituting the perturbative expansions for the eigenvalues

$$\omega = \omega_0 + \varepsilon\omega_1 + \mathcal{O}(\varepsilon^2), \tag{14}$$

where $\omega_0 = \omega_{0\nu_1} = \omega_{0\nu_2}$, and the eigenvector

$$\overrightarrow{w} = \sum_{\nu'=\nu_1,\nu_2} c_{\nu'}\overrightarrow{w}^{(0)}_{\nu'} + \varepsilon\overrightarrow{w}^{(1)} + \mathcal{O}(\varepsilon^2) \tag{15}$$

into Eq. (13) and keeping terms up to $\mathcal{O}(\varepsilon)$ we obtain

$$\left[c^2q_1^2 - (\nu_2 - \nu_1)\Omega\omega_1\right]c_{\nu_1} + \frac{\omega_c^2}{2}(\delta_{\nu_1\nu_2+1} + \delta_{\nu_1\nu_2-1})c_{\nu_2} = 0, \tag{16a}$$

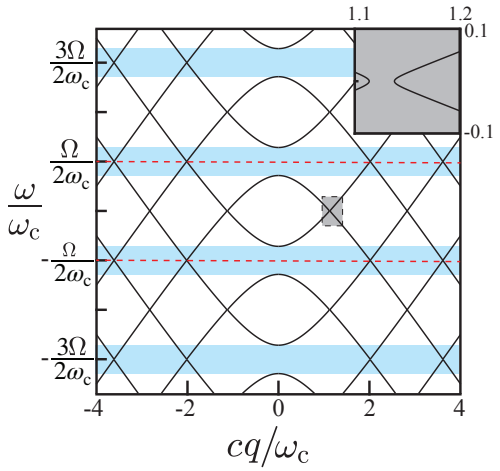

FIG. 2. Dispersion diagram of a Klein-Gordon-type equation featuring a cosinusoidally varying spectral cutoff. The modulation parameters are set to $\Omega = 1.5\omega_c < \Omega_{c1}$ (see below Sec. IV) and $\varepsilon = 0.5$. Horizontal stripes indicate that, in the presence of modulation, the frequency gap is not absolute. Dashed lines represent the edges of the first Brillouin zone. A gray rectangle highlights a second-order crossing of replicas ($\nu_1 = -1$ and $\nu_2 = 1$), resulting in a narrow wavenumber gap, consistent with perturbation theory. An enlarged view of this gap is shown in the inset.

$$\frac{\omega_c^2}{2}(\delta_{\nu_2\nu_1+1}+\delta_{\nu_2\nu_1-1})c_{\nu_1}+\left[c^2q_1^2+(\nu_2-\nu_1)\Omega\omega_1\right]c_{\nu_2}=0. \tag{16b}$$

According to Eqs. (16), mode coupling occurs in first-order perturbation theory when and only when $|\nu_2-\nu_1| = 1$. This behavior is a result of the cosinusoidal modulation choice, restricting first-order coupling to consecutive replicas. However, it is worth noting that there is also higher-order coupling between intersecting replicas of non-consecutive orders. This coupling removes mode degeneracy at the crossing points and results in narrow wavenumber gaps, as illustrated in Fig. 2.

Our analysis will focus on the vicinity of the intersection of consecutive replicas in the dispersion diagram, i.e., around $c^2q_0^2 = \Omega^2/4 - \omega_c^2$, where significant effects are anticipated. In this case, Eqs. (16) can be cast in the form of an eigenvalue-eigenvector problem

$$\begin{pmatrix}\delta & 1\\ -1 & -\delta\end{pmatrix}\begin{pmatrix}c_\nu\\ c_{\nu+1}\end{pmatrix}=\mu\begin{pmatrix}c_\nu\\ c_{\nu+1}\end{pmatrix}, \tag{17}$$

where $\delta = 2c^2q_1^2/\omega_c^2$ and $\mu = 2\Omega\omega_1/\omega_c^2$. The eigenvalues are

$$\mu_\pm = \pm\sqrt{\delta^2-1} \tag{18}$$

and, recalling that $c^2q^2 = c^2q_0^2+\varepsilon c^2q_1^2$ with $c^2q_0^2 = \Omega^2/4-\omega_c^2$ and $\omega = \omega_0+\varepsilon\omega_1$ with $\omega_0 = (2\nu+1)\Omega/2$, we obtain the dispersion relation

$$\omega(q) = (2\nu+1)\frac{\Omega}{2}\pm\frac{1}{\Omega}\sqrt{\left(c^2q^2+\omega_c^2-\frac{\Omega^2}{4}\right)^2-\left(\frac{\varepsilon\omega_c^2}{2}\right)^2}. \tag{19}$$

The associated eigenvectors are given by

$$\begin{pmatrix}c_\nu\\ c_{\nu+1}\end{pmatrix}_\pm = \begin{pmatrix}-\delta\mp\sqrt{\delta^2-1}\\ 1\end{pmatrix}. \tag{20}$$

Therefore, when $\delta^2 \neq 1$, Eq. (5) along with Eqs. (6), (14) and (15), to zeroth order, yield the two linearly independent solutions

$$u_{1,2;q}(t) = \left[e^{i\frac{\Omega}{2}t}-\left(\delta\pm\sqrt{\delta^2-1}\right)e^{-i\frac{\Omega}{2}t}\right]e^{-i\varepsilon\omega_{1\pm}t}. \tag{21}$$

If $\delta^2 = 1$, it is evident from Eq. (18) and Eq. (20) that the two eigenvalues become degenerate and equal to zero ($\omega_1 = 0$), while the corresponding eigenvectors coalesce, as expected since the 2×2 matrix in Eq. (17) becomes defective. Therefore, $\delta^2 = 1$, which implies $\omega_1 = 0$ and thus $\omega = \omega_0$, corresponds to an exceptional point of degeneracy. The coalesced eigenvectors yields a single solution

$$u_{1;q}(t) = e^{i\frac{\Omega}{2}t}\mp e^{-i\frac{\Omega}{2}t}, \tag{22}$$

for $\delta = \pm1$, respectively. The second linearly independent solution at the exceptional point can be obtained with the help of Eqs. (9) and (10), taking the form

$$u_{2;q}(t) = \frac{i\Omega^2}{\varepsilon\pi\omega_c^2}e^{-\frac{i\Omega}{2}t}-\frac{\Omega t}{2\pi}u_{1;q}(t). \tag{23}$$

In any case, the general solution is expressed as a linear combination of $u_{1;q}$ and $u_{2;q}$ with coefficients determined by the initial conditions, requiring continuity of both the field and its first derivative.

When seeking complex-q solutions of the wave equation at a given real frequency ω, perturbative analysis yields

$$\begin{pmatrix}\mu & -1\\ -1 & -\mu\end{pmatrix}\begin{pmatrix}c_\nu\\ c_{\nu+1}\end{pmatrix}=\delta\begin{pmatrix}c_\nu\\ c_{\nu+1}\end{pmatrix}. \tag{24}$$

This equation can also be derived directly, by reformulating Eq. (17) to express δ as the eigenvalue. Equation (24) presents eigenvalues $\delta_\pm = \pm\sqrt{\mu^2+1}$ with associated eigenvectors $(c_\nu, c_{\nu+1})_\pm^{\mathrm{T}} = (\mu\pm\sqrt{\mu^2+1}, 1)^{\mathrm{T}}$, where T denotes vector transpose. Notably, the symmetric form of the 2×2 matrix in Eq. (24) prevents the eigenvectors from coalescing. Eqs. (17) and (24) produce the same dispersion diagram on the real q-ω plane because, in both cases, the dispersion diagram is governed by the same equation, which is solved either with respect to ω (see Eq. (19)) or with respect to q. However, an important distinction arises: the exceptional points in the complex-ω versus real-q representation transform into doubly degenerate points in the complex-q versus real-ω representation, which is in line with recent work [34].

IV. DISCUSSION OF DISPERSION DIAGRAMS

We have already discussed the emergence of exceptional points in our system under consideration when $\omega_1 = 0$. The exceptional points are located either at $q \neq 0$ (at the edges of wavenumber gaps) or at $q = 0$, depending on the modulation frequency. Here, we focus on the latter case, where exceptional points lie at $(q, \omega) = (0, (2\nu + 1)\Omega/2)$. These exceptional points appear at some characteristic (critical) frequencies of the time modulation. In first-order perturbation theory, these frequencies can be directly obtained from Eq. (19), which, for $q = 0$ and $\omega = (2\nu + 1)\Omega/2$, yields

$$\Omega_{c1}^2 = 4\omega_c^2 \left(1 - \frac{\varepsilon}{2}\right), \ \Omega_{c2}^2 = 4\omega_c^2 \left(1 + \frac{\varepsilon}{2}\right). \tag{25}$$

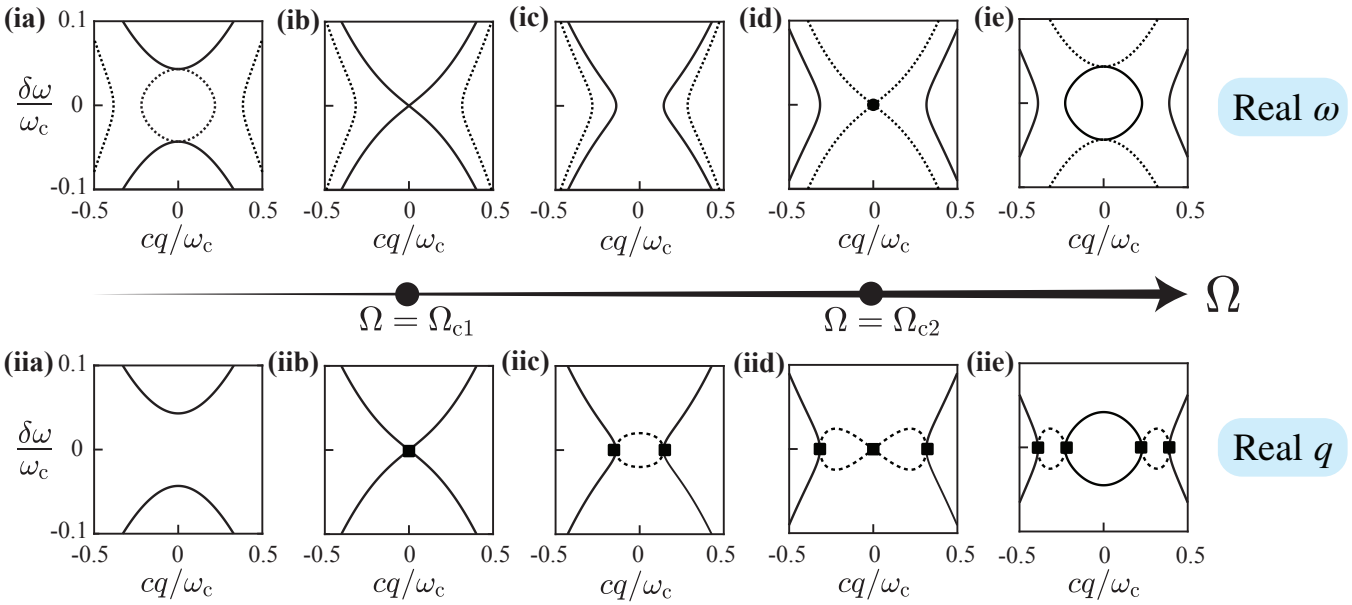

FIG. 3. Evolution of the dispersion diagram, where $\delta\omega = \omega - (2\nu + 1)\Omega/2$, for a Klein-Gordon-type equation featuring a cosinusoidally varying spectral cutoff frequency with a relative amplitude $\varepsilon = 0.1$, versus the modulation frequency Ω. The plots depict the dispersion diagram in the vicinity of two successive interacting replicas and correspond to different values of Ω, presented from left to right as $1.9\omega_c$, Ω_{c1}, $1.97\omega_c$, Ω_{c2}, and $2.1\omega_c$. The top and bottom sequences represent the dispersion diagram in real frequency versus complex wavenumber and complex frequency versus real wavenumber, respectively. Solid lines represent the real parts, while dashed lines represent the imaginary parts of the wavenumber (or frequency) associated with the various bands. The exceptional points in the bottom sequence are denoted by squares.

As depicted in Figs. 1(a) and (b), for $\Omega < \Omega_{c1}$, the real-q branches of consecutive replicas in the dispersion diagram do not intersect, while their imaginary-q branches exhibit two intersections. The interaction of the latter results in two avoided crossings, giving rise to a closed loop on the ω-Im(q) plane, connecting the edges of the real-q branches. However, it is important to clarify that this closed loop does not correspond to an absolute frequency gap, as real-q branches from other replicas are also present in this spectral region, as shown in Fig. 2. In addition, a pair of branches with larger Im(q), symmetrically positioned about $q = 0$, is formed, as depicted in Fig. 3(ia).

As the modulation frequency increases, the edges of the real-q branches approach each other. At $\Omega = \Omega_{c1}$, these branches intersect linearly at $(q, \omega) = (0, (2\nu + 1)\Omega_{c1}/2)$, representing a gapless Dirac dispersion, which at the crossing point hosts an exceptional point. Indeed, as can be readily deduced from Eq. (19) and the first of Eqs. (25), for $q \to 0$

$$\omega(q) \sim (2\nu + 1)\frac{\Omega_{c1}}{2} \pm \frac{\sqrt{\varepsilon}\omega_c}{\Omega_{c1}} cq. \tag{26}$$

Meanwhile, the two branches with larger Im(q) remain relatively unaffected, as seen in Fig. 3(ib).

Beyond Ω_{c1}, the intersecting bands undergo separation, leading to the emergence of an absolute wavenumber gap around $q = 0$, as depicted in Fig. 3(ic). Within this gap, the frequency eigenvalues are complex [see Fig. 3(iic)], signifying waves that either grow or decay exponentially in time. As the modulation frequency increases, the gap widens and, simultaneously, the two branches with larger Im(q) draw closer together. At $\Omega = \Omega_{c2}$, they ultimately converge and exhibit a linear

variation about the convergence point $(q,\omega)=(0,(2\nu+1)\Omega_{c2}/2)$, as shown in Fig. 3(id). Indeed, for $q\to 0$, Eq. (19), in conjunction with the second of Eqs. (25), yields

$$\omega(q)\sim(2\nu+1)\frac{\Omega_{c2}}{2}\pm i\frac{\sqrt{\varepsilon}\omega_c}{\Omega_{c2}}cq\,, \tag{27}$$

which represents an imaginary Dirac dispersion, similar to [34]. At the crossing point, an isolated in-gap state emerges, and the continuous wavenumber gap around $q=0$ breaks into two parts, one at $q<0$ and one at $q>0$, as depicted in Fig. 3(iid). The isolated in-gap state corresponds to an exceptional point.

For modulation frequencies above the second critical value, Ω_{c2}, as illustrated in Figs. 1(c) and (d), the real-q branches of consecutive replicas in the dispersion diagram intersect, while their imaginary-q branches are separated. The interaction of the former results in two avoided crossings, giving rise to three real-q branches, separated by two wavenumber gaps, situated symmetrically about $q=0$. Figs. 3(ie), (iie) provide a visual representation of this dispersion diagram, illustrating the evolution from an isolated in-gap point at $q=0$ to a real-q closed loop around $q=0$ as the modulation frequency increases beyond Ω_{c2}.

Remarkably, the closed-form expression in Eq. (19), derived in first-order perturbation theory, accurately reproduces all dispersion diagrams depicted in Fig. 3, obtained through numerical solution of Eq. (7), with exceptional precision. Notably, the differences are imperceptible at the scale of the figure.

It is worth noting that a distinctive aspect in the discussion of our results pertains to the evolution of dispersion diagrams presented in Fig. 3 when compared to cases where the periodic modulation is applied to the velocity rather than the cutoff frequency. In the latter scenario, assuming a variation of the form $c^2[1+\varepsilon\cos(\Omega t)]$, instead of Eq. (19) we obtain

$$\omega(q)=(2\nu+1)\frac{\Omega}{2} \pm\frac{1}{\Omega}\sqrt{\left(c^2q^2+\omega_c^2-\frac{\Omega^2}{4}\right)^2-\left(\frac{\varepsilon}{2}\left[\omega_c^2-\frac{\Omega^2}{4}\right]\right)^2}\,, \tag{28}$$

predicting a direct transition from the frequency gap shown in Figs. 3(ia) and (iia) to a pair of wavenumber gaps symmetrically situated around $q=0$, as illustrated in Figs. 3(ie) and (iie). At the critical frequency, $\Omega_c=2\omega_c$, we obtain a parabolic dispersion relation instead of a Dirac one, given by

$$\omega(q)=(2\nu+1)\frac{\Omega_c}{2}\pm\frac{c^2q^2}{\Omega_c}\,. \tag{29}$$

Furthermore, at any modulation frequency, the modes at $q=0$ in this case represent trivial oscillations described by $d^2u_q/dt^2+\omega_c^2u_q=0$.

In addition, it should be highlighted that only the dispersion diagrams in Figs. 3(ie) and (iie) are analogous to those of typical temporally modulated wave systems [31, 35, 36]. In this context, it is widely acknowledged that a wave packet, located in q-space within a wavenumber gap in such a dispersion diagram, undergoes amplification due to the excitation of exponentially growing modes [30, 37–40]. However, this is not the only possible scenario for Klein-Gordon media. As discussed earlier, Klein-Gordon media with periodic variations in cutoff frequency exhibit distinctive features. Firstly, they can host wavenumber gaps, either centered around $q=0$ for $\Omega_{c1}<\Omega<\Omega_{c2}$ or around $q\neq 0$ for $\Omega\geq\Omega_{c2}$. Moreover, they can have no such gaps when $\Omega\leq\Omega_{c1}$. This unique behavior enables effective control over the amplification or propagation of a waveform by tuning only the modulation frequency Ω while maintaining a constant modulation amplitude $\varepsilon\neq 0$. Though, their most intriguing feature is the emergence of a gapless Dirac dispersion relation at a singular exceptional point when $\Omega=\Omega_{c1}$. This unprecedented phenomenon significantly influences wave propagation as will be discussed below.

Before proceeding to the numerical investigation, it's noteworthy to mention recent predictions regarding Dirac dispersion, centered at an exceptional point, in systems described by the Schrödinger equation subject to a complex potential [41]. These predictions encompass linear Dirac dispersion in either real or imaginary space [34], similar to our cases for $\Omega=\Omega_{c1}$ and $\Omega=\Omega_{c2}$, respectively. Nevertheless, these so-called Dirac exceptional points are defined in a hybrid space consisting of a momentum dimension and a synthetic dimension for the strength of non-Hermiticity [34, 41]. In this respect, they are distinctly different from both typical Dirac points, commonly associated with diabolic points [42], which may arise accidentally or due to symmetry in non-Hermitian systems similar to those in Hermitian systems, and the conventional exceptional points.

V. TIME INTERFACES

We now present numerical results to illustrate various phenomena related to wave dynamics in the system under consideration, with particular emphasis on the case with modulation frequency $\Omega=\Omega_{c1}$, at the exceptional point. For our numerical simulations, we solve Eq. (1) using a finite-difference scheme for the spatial differentiation and a fourth-order Runge-Kutta method for the time evolution. The spatial domain is chosen to be $L=200c/\omega_c$ and we apply periodic boundary conditions. For illustration purposes, we consider scattering at a time interface, assuming

$$\widetilde{\omega}_c^2(t)=\begin{cases}\omega_c^2, & t<0\\ \omega_c^2[1+\varepsilon\cos(\Omega t)], & t\geq 0.\end{cases} \tag{30}$$

while the numerical simulation is initiated at $t=t_0<0$.

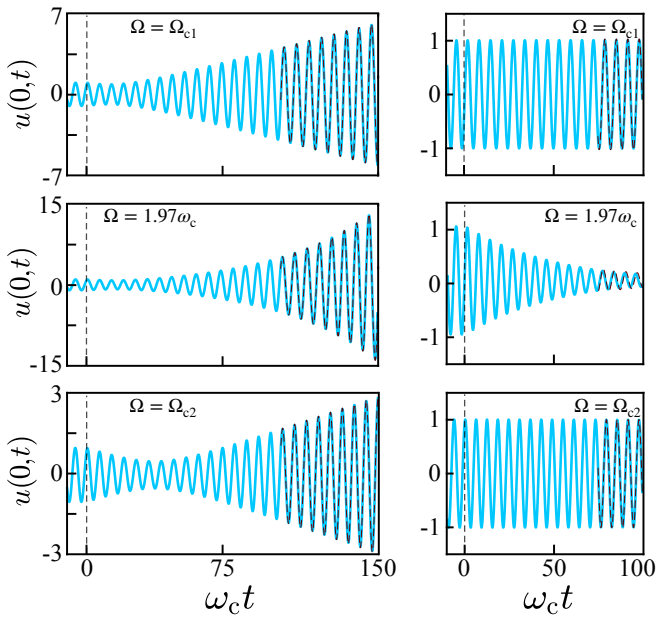

FIG. 4. Time evolution of a spatially homogeneous solution to a Klein-Gordon-type equation, initiated at $\omega_c t_0 = -10$, with a cosinusoidal modulation of the cutoff frequency activated at $t = 0$ according to Eq. (30). The relative amplitude of the modulation is $\varepsilon = 0.1$ and we focus on three characteristic modulation frequencies: Ω_{c1}, $1.97\omega_c$, and Ω_{c2}. The diagrams in the left-hand panel correspond to a phase parameter $\phi = \pi/3$ while in the right-hand panel ϕ is chosen to prevent excitation of the unstable solutions according to perturbation theory ($\phi = 0$ for $\Omega = \Omega_{c1}$, $\phi \approx 0.4768$ for $\Omega = 1.97\omega_c$, and $\phi = \pi/2$ for $\Omega = \Omega_{c2}$). The solid and dashed curves show the numerical and the perturbation theory results, respectively, highlighting the remarkable agreement between the two.

A. Spatially Uniform Fields

The analysis presented in the previous section reveals particular interest in the properties of Klein-Gordon media with a periodic cutoff frequency variation around $q = 0$, i.e. spatially uniform field profiles. At this specific point, as we have already discussed in Sec. II and Sec. III, we have (i) two stable periodic solutions if $\Omega < \Omega_{c1}$ or $\Omega > \Omega_{c2}$ since $\omega \in \mathbb{R}$, (ii) one stable periodic solution and one linearly growing if $\Omega = \{\Omega_{c1}, \Omega_{c2}\}$ due to the presence of the exceptional point, and (iii) one growing and one decaying exponentially in time solution if $\Omega_{c1} < \Omega < \Omega_{c2}$ since $\omega \in \mathbb{C}$. For the aforementioned cases, the perturbative analysis of Sec. III allows us to derive exact expressions, in zeroth order of the field $u(x,t)$ for $t \geq 0$. These solutions are uniquely defined by $u(x,0)$ and $u_t(x,0)$, where the subscript t denotes the partial derivative with respect to time.

For $t < 0$, the solution to Eq. (1) for a spatially uniform field ($q = 0$), of unit amplitude, can be expressed as $u(x,t) = \sin(\omega_c t + \phi)$ and the initial conditions read $u(x,t_0) = \sin(\omega_c t_0 + \phi)$ and $u_t(x,t_0) = \omega_c \cos(\omega_c t_0 + \phi)$. At $t = 0$, when the modulation is activated, we have $u(x,0) = \sin\phi$ and $u_t(x,0) = \omega_c \cos\phi$, which allows us to obtain the perturbative solution in terms of the single phase parameter ϕ. Figure 4 illustrates that this approximate solution effectively captures the time evolution of the field in both linearly and exponentially unstable operating regimes. This is demonstrated by comparing the perturbative results with numerically obtained ones.

Hence, due to the accuracy of the perturbation method, we can estimate the initial conditions in which the unstable eigenmode will not be excited, as illustrated in Fig. 4. However, it is important to note that, in general, the presence of small noise or perturbations will eventually excite the unstable modes that will dominate over an extended period of time.

B. Gaussian wave packets localized around the Dirac point

As detailed in Sec. V A and Fig. 4, stable time evolution can be achieved if $u_{q=0}(0) = 0$. Consequently, a wave packet, initially well-localized around $q = 0$ in the q-space, will split into two counter-propagating components, moving at constant opposite velocities $d\omega/dq = \pm\sqrt{\varepsilon}c\omega_c/\Omega_{c1}$. This stands in stark contrast to commonly studied periodically modulated wave systems, where moving wave packets, with Fourier components located in q-space near the unstable wavenumber region, undergo amplification upon activation of modulation.

In agreement with the above analysis, in Fig. 5 we show that, indeed, the excitation of the unstable mode can be avoided. Namely, we consider a sufficiently wide Gaussian initial wave packet, described by $u(x,t_0) = \exp[-(\omega_c x/15c)^2]\sin(\omega_c t_0 + \phi)$ with $u_t(x,t_0) = \omega_c \exp[-(\omega_c x/15c)^2]\cos(\omega_c t_0 + \phi)$. This specific wave packet form implies that its $q = 0$ Fourier component, evolving over time, becomes proportional to $\sin\phi$ when temporal modulation is initiated at $t = 0$. Consequently, as illustrated in Figs. 5(a) and (b), for $\phi = 0$, excitation of the (linearly) unstable mode is prevented and the initially stationary wave packet splits into two. The strong localization of the wave packet in q-space around $q = 0$ ensures the propagation of the two split wave packets with constant group velocities $v_g = \pm\sqrt{\varepsilon}\omega_c c/\Omega_{c1}$ corresponding to a dispersionless propagation, as expected from the linear Dirac dispersion relation.

Contrary to this pattern, Fig. 6 reveals the manifestation of the unstable mode when ϕ is set to a non-zero value, here chosen to be $\phi = \pi/2$. However, despite the expected uniform linear amplitude growth, such behavior is not observed. As shown in Figs. 6(b) and (c), the wave packet adopts a square shape, with its width expanding at a constant speed equal to the wave speed at the Dirac point, $v_g = \sqrt{\varepsilon}\omega_c c/\Omega_{c1}$. Meanwhile, its amplitude tends to saturate. Similar phenomena have been encountered in the diffraction of wave packets in complex crystals, where spectral singularities emerge at the

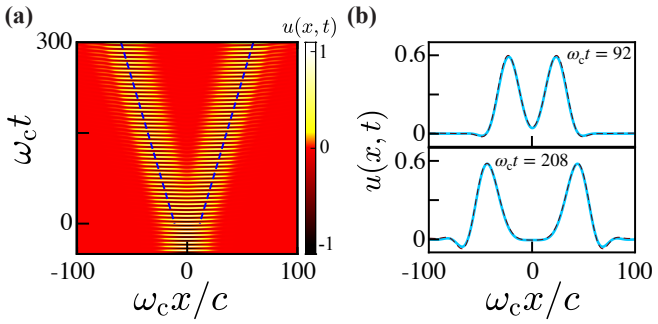

FIG. 5. Evolution of a Gaussian wave packet, described by $u(x,t_0) = \exp\left[-(\omega_c x/15c)^2\right]\sin(\omega_c t_0+\phi)$, $u_t(x,t_0) = \omega_c \exp\left[-(\omega_c x/15c)^2\right]\cos(\omega_c t_0+\phi)$ and launched at $\omega_c t_0 = -50$ in a Klein-Gordon medium with cosinusoidal modulation of the cutoff frequency, activated at $t=0$ according to Eq. (30). The relative modulation amplitude is $\varepsilon = 0.1$, the modulation frequency is $\Omega = \Omega_{c1}$ and the phase parameter $\phi = 0$ prevents excitation of the unstable mode, as illustrated in (a), resulting in two wave packets propagating in opposite directions with constant velocities $d\omega/dq = \pm\sqrt{\varepsilon}\omega_c c/\Omega_{c1}$, as indicated by the dashed lines. Corresponding snapshots of the wave field are presented in (b), calculated numerically (solid curves) and perturbatively (dashed curves).

$\mathcal{PT}$-symmetric-breaking point [43, 44].

In Figs. 5(b) and 6(c) we also compare numerically obtained field profiles with those calculated using perturbative expressions, at selected snapshots. Remarkably, excellent agreement is observed between the two sets of results. To compute the wave packet evolution based on our perturbation theory, we initially calculate the Fourier transforms of $u(x,0)$ and $u_t(x,0)$. These transforms provide the necessary conditions to uniquely define the time evolution of each $u_q(t)$.

The dynamics of wave packets described above can also be elucidated through simple analytical calculations within the framework of our perturbation theory. In the context of the sufficiently wide initial wave packet we consider here, the Fourier coefficients decay rapidly with respect to q. Moreover, for $\Omega = \Omega_{c1}$ we have $\delta = 1 + 2c^2q^2/(\varepsilon\omega_c^2)$. Therefore, assuming $2c^2q^2/(\varepsilon\omega_c^2) \ll 1$, we get $\delta \pm \sqrt{\delta^2-1} \approx 1 \pm 2c|q|/(\sqrt{\varepsilon}\omega_c)$. Substituting this expression into Eq. (21) and considering the general solution $u_q(t) = A_q u_{1;q}(t) + B_q u_{2;q}(t)$, for given initial conditions $u_q(0) \neq 0$ and $\dot{u}_q(0)$, by straightforward calculation we obtain to leading order, $\mathcal{O}(1/q)$, $B_q = -A_q = \sqrt{\varepsilon}\omega_c u_q(0)/(4c|q|)$ for $q \neq 0$. Similarly, for $q=0$, using Eqs. (22) and (23) we get $B_q = -i\varepsilon\pi\omega_c^2 u_q(0)/\Omega_{c1}^2$. In accordance with the order of approximation established in the previous case ($q \neq 0$), we will focus solely on the linearly growing term in the general solution here, which dominates the dynamics over extended periods. This approach yields the following expression for $u_q(t)$, encompassing both cases: $q \neq 0$ and $q = 0$

$$u_q(t) = -\frac{\sqrt{\varepsilon}\omega_c u_q(0)}{c|q|}\sin\left(v_g|q|t\right)\sin\left(\frac{\Omega_{c1}t}{2}\right), \qquad (31)$$

where $v_g = \sqrt{\varepsilon}\omega_c c/\Omega_{c1}$ is the wave speed at the Dirac point. Equation (31) has the form of a rapid oscillation, $\sin(\Omega_{c1}t/2)$, modulated by a slowly varying envelope function. If $u_q(0) = 0$, instead of Eq. (31) we obtain

$$u_q(t) = \frac{2\dot{u}_q(0)}{\Omega_{c1}}\cos\left(v_g|q|t\right)\sin\left(\frac{\Omega_{c1}t}{2}\right). \qquad (32)$$

Let us assume a sufficiently wide Gaussian wave packet of the form $u(x,t_0) = \exp(-x^2/\sigma^2)\sin\phi$ with $u_t(x,t_0) = \omega_c\exp(-x^2/\sigma^2)\cos\phi$, which, for simplicity, is launched in the modulated Klein-Gordon medium at $t_0 = 0$. In this case we have $u_q(0) = \sigma\sqrt{\pi}\exp(-\sigma^2q^2/4)\sin\phi$ and $\dot{u}_q(0) = \omega_c\sigma\sqrt{\pi}\exp(-\sigma^2q^2/4)\cos\phi$. Substituting these initial conditions, for $\phi \neq 0$ and $\phi = 0$, into Eq. (31) and Eq. (32), respectively, the inverse Fourier transform, $u(x,t) = (2\pi)^{-1}\int_{-\infty}^{\infty} dq u_q(t)\exp(iqx)$, can be evaluated

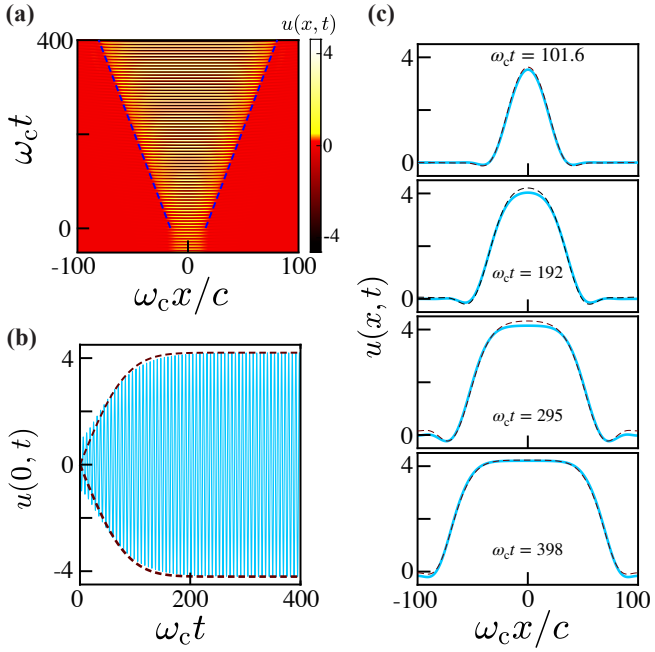

FIG. 6. Evolution of a Gaussian wave packet, described by $u(x,t_0) = \exp\left[-(\omega_c x/15c)^2\right]\sin(\omega_c t_0+\phi)$, $u_t(x,t_0) = \omega_c\exp\left[-(\omega_c x/15c)^2\right]\cos(\omega_c t_0+\phi)$ and launched at $\omega_c t_0 = -50$ in a Klein-Gordon medium with cosinusoidal modulation of the cutoff frequency, activated at $t=0$ according to Eq. (30). The relative modulation amplitude is $\varepsilon = 0.1$, the modulation frequency is $\Omega = \Omega_{c1}$ and the phase parameter $\phi = \pi/2$ maximally excites the unstable mode, as illustrated in (a). The dashed lines indicate the increasing width of the wave packet. Their slope is $d\omega/dq = \pm\sqrt{\varepsilon}\omega_c c/\Omega_{c1}$ as predicted by the Dirac dispersion relation. In (b) the numerically obtained time evolution of $u(0,t)$ (solid curves) is compared with that given by the envelope function in Eq. (33) for $x=0$ (dashed curves), while in (c) corresponding snapshots of the wave field, calculated either numerically (solid curves) or perturbatively (dashed curves), are presented.

analytically yielding

$$u(x,t) = \sqrt{\pi\varepsilon}\frac{\sigma\omega_c}{4c}\sin\phi\left[\mathrm{erf}\left(\frac{x-v_g t}{\sigma}\right) - \mathrm{erf}\left(\frac{x+v_g t}{\sigma}\right)\right] \times \sin\left(\frac{\Omega_{c1}t}{2}\right) \tag{33}$$

for $\phi \neq 0$ and

$$u(x,t) = \frac{\omega_c}{\Omega_{c1}}\left[e^{-(x-v_g t)^2/\sigma^2} + e^{-(x+v_g t)^2/\sigma^2}\right]\sin\left(\frac{\Omega_{c1}t}{2}\right) \tag{34}$$

for $\phi = 0$. The closed-form expressions derived in Eqs. (33) and (34) elucidate the fundamental characteristics governing the dynamics of wave packets associated with the Dirac point, as previously discussed. In particular, when the unstable mode remains unexcited, Eq. (34) clearly illustrates the emergence of two Gaussian beams, propagating without dispersion in opposite directions with constant velocities, equal to the wave speed at the Dirac point. On the other hand, upon exciting the unstable mode, the combination of the two error functions in Eq. (33) has the form of a Heaviside step function, $\sim -2\Theta(v_g t - |x|)$, albeit with rounded edges. This accurately accounts for the observed spreading of the wave packet. Saturation of the wave amplitude is also predicted to the value $[\sqrt{\pi\varepsilon}\sigma\omega_c/(2c)]\sin\phi$. In particular, at $x = 0$, Eq. (33) yields $u(0,t) = -[\sqrt{\pi\varepsilon}\sigma\omega_c/(2c)]\sin\phi\ \mathrm{erf}(v_g t)\sin(\Omega_{c1}t/2)$, in very good agreement with our numerical calculations.

VI. SUMMARY AND CONCLUSION

In summary, our study presents a comprehensive exploration of wave dynamics in time-periodic homogeneous media, governed by a Klein-Gordon-type equation subjected to temporal modulation of either its cutoff frequency or velocity constant. Through a combination of numerical simulations and analytical calculations utilizing perturbation theory, we have elucidated distinct effects arising from these modulations.

Our findings demonstrate that while variations in velocity produce relatively minor effects, modulation of the cutoff frequency yields a rich variety of wave phenomena. Specifically, by appropriately tuning the modulation frequency, we observe the transformation of the intrinsic Klein-Gordon frequency gap into wavenumber gaps, centered at $q = 0$ or symmetrically positioned at $q > 0$ and $q < 0$. At these transitions, we reveal the emergence of Dirac dispersion with exceptional point of degeneracy at $q = 0$, manifesting either in real or imaginary space. In the latter case, we essentially have an isolated in-gap state.

This novel behavior affords effective control over waveform amplification or propagation. Notably, we observe that, with precise adjustment of modulation phase, wave packets localized around the Dirac point, in the real-space dispersion case, undergo intriguing transformations. They either split into counter-propagating wavepackets moving at constant opposite velocities or exhibit spreading at a constant speed with their amplitude saturating. Furthermore, our study provides a coherent interpretation of the underlying mechanisms, supported by simple, analytical closed-form formulas that accurately replicate our results, thus offering valuable physical insights.

In conclusion, our work advances our understanding of wave dynamics in periodically modulated media. The nuanced control over wave properties uncovered in this study holds promise for the development of innovative technologies and theoretical frameworks in various scientific disciplines.

VII. ACKNOWLEDGEMENTS

The authors would like to thank V. Pagneux for fruitful discussions. A.P. and G.T. acknowledge the support from ANR project ExFLEM ANR-21-CE30-0003-01. V.A. is supported by EU H2020 ERC StG “NASA” Grant Agreement No. 101077954.

[1] O. Klein, Zeitschrift für Physik **37**, 895 (1926).
[2] W. Gordon, Zeitschrift für Physik **40**, 117 (1926).
[3] H. Lamb, Proceedings of the Royal Society of London. Series A, Containing papers of a mathematical and physical character **93**, 114 (1917).
[4] N. Marinescu, Progress in quantum electronics **16**, 183 (1992).
[5] A. Banos, W. Mori, and J. Dawson, IEEE transactions on plasma science **21**, 57 (1993).
[6] Z. Musielak, J. Fontenla, and R. Moore, Physics of Fluids B: Plasma Physics **4**, 13 (1992).
[7] B. J. Forbes, E. R. Pike, and D. B. Sharp, The Journal of the Acoustical Society of America **114**, 1291 (2003).
[8] P. Gravel and C. Gauthier, American Journal of Physics **79**, 447 (2011).
[9] Y. Taroyan and R. Erdélyi, Helioseismology, Asteroseismology, and MHD Connections , 521 (2008).
[10] E. Galiffi, R. Tirole, S. Yin, H. Li, S. Vezzoli, P. A. Huidobro, M. G. Silveirinha, R. Sapienza, A. Alù, and J. Pendry, Advanced Photonics **4**, 014002 (2022).
[11] D. Holberg and K. Kunz, IEEE Transactions on Antennas and Propagation **14**, 183 (1966).
[12] F. Biancalana, A. Amann, A. V. Uskov, and E. P. O'reilly, Physical Review E **75**, 046607 (2007).
[13] J. Reyes-Ayona and P. Halevi, Applied Physics Letters **107** (2015).

[14] N. W. Ashcroft and N. Mermin, Physics (New York: Holt, Rinehart and Winston) Appendix C (1976).

[15] S. John, D. Joannopoulos, J. N. Winn, and R. D. Meade, InPrinceton University of Press: Princeton, NJ, USA (2008).

[16] V. Laude, *Phononic crystals: artificial crystals for sonic, acoustic, and elastic waves* (Walter de Gruyter GmbH & Co KG, 2020).

[17] J. C. Slater, Reviews of modern physics **30**, 197 (1958).

[18] E. S. Cassedy and A. A. Oliner, Proceedings of the IEEE **51**, 1342 (1963).

[19] E. S. Cassedy, Proceedings of the IEEE **55**, 1154 (1967).

[20] J. Pendry, E. Galiffi, and P. Huidobro, JOSA B **38**, 3360 (2021).

[21] Y. Yu and G. Shvets, Physical Review B **105**, 195116 (2022).

[22] Y. Sharabi, A. Dikopoltsev, E. Lustig, Y. Lumer, and M. Segev, Optica **9**, 585 (2022).

[23] J. Park, H. Cho, S. Lee, K. Lee, K. Lee, H. C. Park, J.-W. Ryu, N. Park, S. Jeon, and B. Min, Science advances **8**, eabo6220 (2022).

[24] G. Teschl, *Ordinary differential equations and dynamical systems*, Vol. 140 (American Mathematical Soc., 2012).

[25] H. Kazemi, M. Y. Nada, T. Mealy, A. F. Abdelshafy, and F. Capolino, Physical Review Applied **11**, 014007 (2019).

[26] H. Kazemi, M. Y. Nada, A. Nikzamir, F. Maddaleno, and F. Capolino, Journal of Applied Physics **131** (2022).

[27] J. Li, Y. Jing, and S. A. Cummer, Physical Review B **105**, L100304 (2022).

[28] M. Salehi, M. Memarian, and K. Mehrany, Optics Express **31**, 2911 (2023).

[29] M. S. P. Eastham, *The spectral theory of periodic differential equations* (Scottish Academic Press, 1973).

[30] M. Lyubarov, Y. Lumer, A. Dikopoltsev, E. Lustig, Y. Sharabi, and M. Segev, Science **377**, 425 (2022).

[31] J. R. Zurita-Sánchez, P. Halevi, and J. C. Cervantes-Gonzalez, Physical Review A **79**, 053821 (2009).

[32] A. Paliovaios and N. Stefanou, Phys. Rev. B **106**, 024101 (2022).

[33] N. Stefanou, I. Stefanou, E. Almpanis, N. Papanikolaou, P. Garg, and C. Rockstuhl, J. Opt. Soc. Am. B **40**, 2842 (2023).

[34] J. H. Rivero, L. Feng, and L. Ge, Physical Review B **107**, 104106 (2023).

[35] G. Trainiti, Y. Xia, J. Marconi, G. Cazzulani, A. Erturk, and M. Ruzzene, Physical review letters **122**, 124301 (2019).

[36] S. Lee, J. Park, H. Cho, Y. Wang, B. Kim, C. Daraio, and B. Min, Photonics Research **9**, 142 (2021).

[37] T. T. Koutserimpas, A. Alù, and R. Fleury, Physical Review A **97**, 013839 (2018).

[38] D. Torrent, W. J. Parnell, and A. N. Norris, Physical Review B **97**, 014105 (2018).

[39] B. L. Kim, C. Chong, S. Hajarolasvadi, Y. Wang, and C. Daraio, Physical Review E **107**, 034211 (2023).

[40] J. S. Martínez-Romero and P. Halevi, Physical Review A **96**, 063831 (2017).

[41] J. H. Rivero, L. Feng, and L. Ge, Physical Review Letters **129**, 243901 (2022).

[42] H. Xue, Q. Wang, B. Zhang, and Y. Chong, Physical Review Letters **124**, 236403 (2020).

[43] S. Longhi, Physical Review A **81**, 022102 (2010).

[44] E.-M. Graefe and H. Jones, Physical Review A **84**, 013818 (2011).